ADVANCED FUNCTIONAL MATERIALS
www.afm-journal.de

Cell Activities on Viscoelastic Substrates Show an Elastic Energy Threshold and Correlate with the Linear Elastic Energy Loss in the Strain-Softening Region

Francesco Piazza, Pasquale Sacco, Eleonora Marsich, Gabriele Baj, Francesco Brun, Fioretta Asaro, Gabriele Grassi, Mario Grassi, and Ivan Donati*

Energy-sensing in viscoelastic substrates has recently been shown to be an important regulator of cellular activities, modulating mechanical transmission and transduction processes. Here, this study fine-tunes the elastic energy of viscoelastic hydrogels with different physical and chemical compositions and shows that this has an impact on cell response in 2D cell cultures. This study shows that there is a threshold value for elastic energy (≈0.15 J m^{-3}) above which cell adhesion is impaired. When hydrogels leave the linear stress–strain range, they show softening (plastic) behavior typical of soft tissues. This study identifies a correlation between the theoretical linear elastic energy loss in the strain-softening region and the number of cells adhering to the substrate. This also has implications for the formation of vinculin-rich anchorage points and the ability of cells to remodel the substrate through traction forces. Overall, the results reported in this study support that the relationship between cell activities and energy-sensing in viscoelastic substrates is an important aspect to consider in the development of reliable ex vivo models of human tissues that mimic both normal and pathological conditions.

1. Introduction

Viscoelasticity is an almost universal property of living tissues and extracellular matrices (ECMs).[1] In response to a mechanical stimulation, viscoelastic tissues exhibit an immediate elastic response characteristic of purely elastic solids, followed by a viscous energy dissipation characteristic of viscous fluids. Beside elasticity, viscoelasticity is increasingly recognized as an important regulator of cell activity.[2–10]

In biological terms, cells probe the surrounding ECM through volume expansion or via the "molecular clutch machinery," i.e., the myosin-actin-integrin axis.[3,11] In the latter case, myosin contractility drives a continuous retrograde flow of actin toward the center of the cell, sensing through the integrins the elastic resistance of the ECM to deformation. For almost elastic materials, the high loading rate allows the force-sensitive protein talin to unfold before the integrin-ECM link breaks, leading to vinculin binding, adhesion site growth, and downstream signaling.[12] Given the viscoelastic nature of living tissues, the molecular clutch model has been generalized by introducing dissipative contributions, revealing that viscosity mediates via the same talin unfolding mechanism.[13] Strikingly, it was found that viscosity can compensate for reduced elasticity if the relaxation of stresses generated by cells is fast.[14] The amount of viscous energy dissipated is tissue-dependent, so tissues such as the brain can dissipate at least as much energy as they store in elastically recoverable deformations.[1]

Viscous energy dissipation can be determined under loading/unloading stress–strain cycles (hysteresis area) or

F. Piazza, P. Sacco, G. Baj, G. Grassi, I. Donati
Department of Life Sciences
University of Trieste
Via Licio Giorgieri 5, I-34127 Trieste, Italy
E-mail: psacco@units.it

The ORCID identification number(s) for the author(s) of this article can be found under https://doi.org/10.1002/adfm.202307224

DOI: 10.1002/adfm.202307224

E. Marsich
Department of Medicine
Surgery and Health Sciences
University of Trieste
Piazza dell'Ospitale 1, I-34129 Trieste, Italy

F. Brun, M. Grassi
Department of Engineering and Architecture
University of Trieste
Via A. Valerio 6/1, I-34127 Trieste, Italy

F. Asaro
Department of Chemical and Pharmaceutical Sciences
University of Trieste
Via Licio Giorgieri 1, I-34127 Trieste, Italy

by calculating the loss tangent through rheometry.[2,10,15] Soft but also stiffer tissues exhibit viscous moduli that are generally 10% to 20% of their elastic moduli, i.e., loss tangents in the range of 0.1–0.2. Apart from viscous energy dissipation, it has recently been shown that cells exhibit elastic energy-sensing that affects important biological functions mediated by the same molecular clutch machinery. This material trait can be specifically manipulated by releasing weak physical entanglements or introducing energy dampers.[16,17] Thus, the easier the escape from the linear stress–strain response (and the subsequent entry into the plastic region), the more biological processes of mechanotransduction are activated in 2D cell cultures.

This evidence seems to point to the presence of an elastic energy threshold for viscoelastic substrates that cells must overcome to transduce specific biophysical cues, but whether and how it correlates with specific cell functions is unclear. Here, we have fabricated viscoelastic substrates from agaroses with varying chemical and physical composition showing very low viscous energy dissipation (low loss tangents, in the range 4–6%) and suitable for 2D cell culture to investigate the effect of the elastic energy determined by oscillatory shear on cell behavior. First, we were able to demonstrate that there is a threshold value for the elastic energy above which the adhesion to the substrate is prohibited for cells of different origins. Secondly, the easier the entering into the nonlinear (strain softening) region, the higher the theoretical linear elastic energy loss generated by the oscillatory shear. This type of energy correlates with cell activities in terms of adhesion to the substrate, mechanotransduction of biophysical cues and ECM remodeling caused by cell traction forces.

2. Results

2.1. Methylation Pattern in Agarose Regulates the Linear Stress–Strain Region, Discouraging Cell Adhesion

In the present work, three agarose samples from *Gracilaria*, *Gelidium* and agarose for electrophoresis (EP), which have a low content of agaropectins (Appendix S2, Table S1, Supporting Information), were considered. Molecular differences between the samples concern the amount and pattern of methyl groups along the chain and molecular weight. The NMR analyses allow the identification of the signals of the two sugars (D-galactose and 3,6-anhydro-L-galactopyranose) that compose the agarose (disaccharide) repeating unit (Figures S1–S3, Supporting Information). While the NMR signals of the repeating unit overlap, a close examination of the 3.3–3.6 ppm range reveals differences in methylation between the three samples (**Figure 1**a and Figure S4, Supporting Information). ^{1}H-, ^{13}C-HSQC spectra allow determination of the methylation pattern for the three samples (Figure 1a and Figures S5–S7, Supporting Information). The EP sample shows methylation on G6 of agarose repeating unit. The signal 3.43 ppm; 61.4 ppm is assigned to the methoxy group on G6, while the signal at about 3.70 ppm; 74.2 ppm corresponds to the two protons on G6. The analyses performed on agarose from *Gelidium* show the presence of two methylation sites, G6 and A2, respectively. The methoxy group of the latter appears at 3.52 ppm; 61.4 ppm. In the ^{1}H-, ^{13}C-HSQC, two additional peaks are detected: 3.81 ppm; 81.2 ppm, assigned to the protons of A2 of the methylated disaccharide. 5.19 ppm; 101.1 ppm, which belong to the proton of A1 of the methylated disaccharide. In the agarose samples of *Gracilaria*, in addition to the methylation at G6, the peak at about 3.44 ppm; 64.1 ppm is assigned to the methoxy group at G4. Interestingly, the three agarose samples exhibit different amount and pattern of methylation (Table in Figure 1a). The complete assignments of the methylated disaccharides in the three agarose samples are listed in the Appendix S1 (Supporting Information).

The agarose samples from *Gelidium* and EP have similar shear viscosity (η) and thus similar molar mass (M) ($\eta = N^{3.4} = M^{3.4}$ where N is the number of repeating units in the polysaccharide chain),[18,19] while a slightly higher value was found for the agarose from *Gracilaria* (Figure 1b). The gelling temperature measured by the hard shaking method seems to correlate more with the viscosity and thus the molar mass than with the presence of methyl residues along the chain (Figure 1c). Collectively, this evidence suggests a different degree and pattern of methylation in the three agarose samples examined.

Next, we mechanically analyzed hydrogels from agaroses of different sources dispersed in PBS buffer that were produced by temperature-assisted gelation (**Figure 2**a).[20] Figure 2b shows the initial elastic modulus determined by uniaxial compression for 1% (w/V) hydrogels of the three agarose hydrogels considered. The presence of methoxy groups does not significantly affect the elastic response of the hydrogel networks, albeit a mild decrease is observed for *Gelidium* sample. Additional mechanical characterizations were carried out on hydrogels from different agarose source. The time required to halve the initial stress, i.e., $\tau_{1/2}$ (Appendix S3, Supporting Information), is not statistically different for the three samples considered (Figure 2c), meaning that the hydrogels exhibit the same viscoelasticity. However, differences among the three agarose samples emerge when shear stress is applied, as shown by the trend in critical strain, γ_{crit}, (Figure 2d). The latter is defined as the strain at which the linear stress–strain relationship is lost for the hydrogel sample (Appendix S4, Supporting Information). While the hydrogel from EP agarose has a very low value of critical strain, larger γ_{crit} values are measured for agarose from *Gelidium* and *Gracilaria*. This leads to a significant difference in the linear elastic energy, E_e (Equation 1)[16,17] for the three hydrogel samples (Figure 2e). E_e is defined as the total energy stored by the material in the linear deformation range, which extends from $\gamma = 0$ to γ_{crit}:

$$E_e = \int_{\gamma=0}^{\gamma_{crit}} \left(\left. \frac{d\sigma}{d\gamma} \right|_{\gamma=0} \right) \gamma \, d\gamma = \frac{1}{2} G_0 \gamma_{crit}^2 \quad (1)$$

Considering the different amount and spatial distribution of methyl groups in the three agarose samples examined, we conclude that the chemical composition of agarose plays a key role in influencing the elastic energy that can be stored by the material in the linear stress–strain regime.[21,22] This parallels the effect of acetyl groups within chitosan hydrogels[16] and of the physical entanglements throughout semi-interpenetrating networks.[17] When MG63 (human osteosarcoma cell line) are plated on these hydrogels they adhere to and spread on hydrogels of EP agarose, while *Gelidium* and *Gracilaria* hydrogels behave as nonpermissive substrates (Figure 2f). Considering that all agarose hydrogels have the same elastic modulus, viscoelasticity, and protein density on the surface (Figure S17, Supporting Information), this

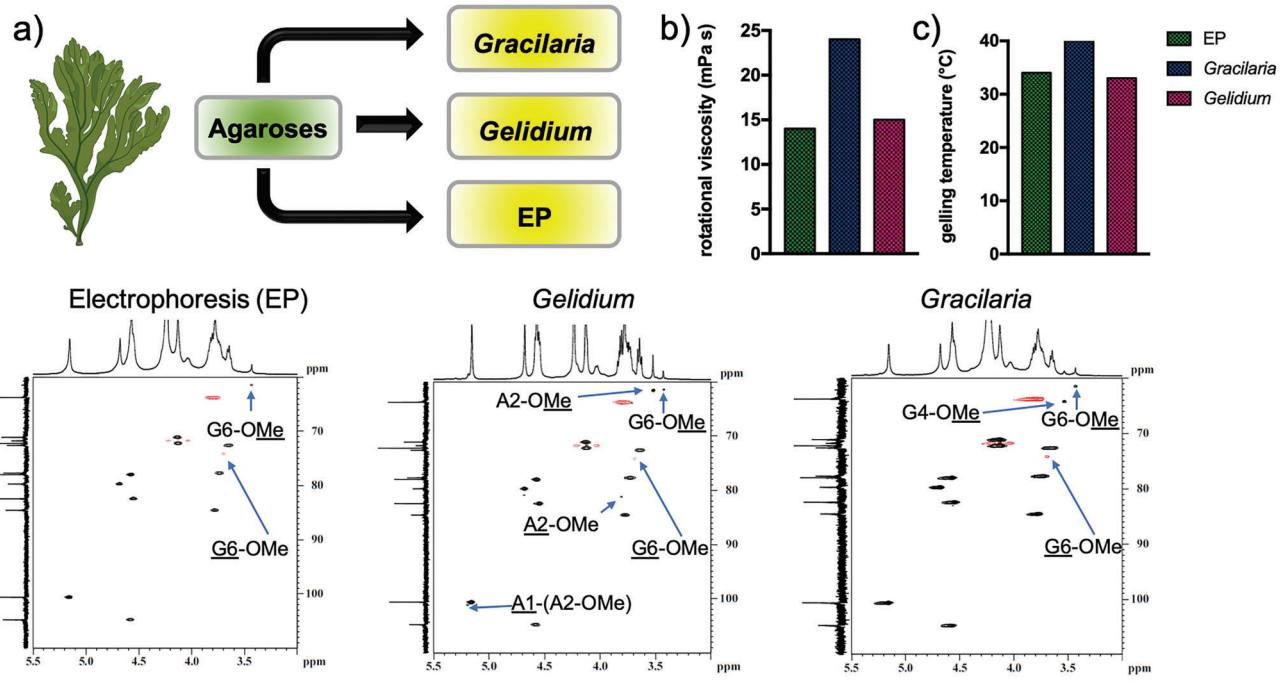

	G6-OMe	A2-OMe	G4-OMe	Total methylation
EP	7.4%	-	-	7.4%
Gracilaria	7.0%	-	5.8%	12.8%
Gelidium	4.3%	11.2%	-	15.5%

Figure 1. Agaroses from different sources show different chemical composition and physical properties. a) The agaroses used in this study are from different sources. One is a standard agarose used for electrophoresis (EP) and the others are agaroses from the seaweeds *Gelidium* and *Gracilaria*. Overall, the repeating unit consists of the disaccharide D-galactose (G unit) and 3,6-anhydro-L-galactopyranose (A unit). The agaroses have been analyzed by ^{1}H- and ^{13}C-HSQC to verify residual methylation: G6-OMe represents the signal of the methoxy group on carbon 6 of the G residue while G6-OMe represents the signal of the two protons on carbon 6 of the methylated G residue. A2-OMe represents the signal of the methoxy group on carbon 2 of the A residue while A2-OMe and A1-(A2-OMe) represent the signals of the protons on carbon 2 and on carbon 1, respectively, of the methylated A residue. G4-OMe represents the signal of the methoxy group on carbon 4 of the G residue while G4-OMe represents the signal of the proton on carbon 4 of the methylated G residue. The table summarizes the degree and pattern of methylation for the three agaroses analyzed. b) Rotational viscosity and c) gelling temperature for the three agaroses used in this study.

suggests that the extent of linear elasticity could play an important role in controlling cell adhesion.

2.2. Identification of the Elastic Energy Threshold that Determines Cell Adhesion

We prepared hydrogels with different concentrations of EP agarose, and agarose of *Gelidium* and *Gracilaria*. While all EP hydrogels with different polymer concentration relax the stress rapidly and have similar $\tau_{1/2}$ (Figure S13, Supporting Information), shear modulus, critical strain, and linear elastic energy differ (**Figure 3**a-c). Cell adhesion of MG63 does not appear to correlate with either critical strain or shear modulus (Figure 3a,b). Of note, a 0.5% w/V EP agarose hydrogel allows cell adhesion despite a higher critical strain and lower shear modulus than a 1% w/V agarose hydrogel of both *Gracilaria* and *Gelidium*. When correlating cell adhesion with the linear elastic energy a pattern emerges (Figure 3d,e). Strikingly, all hydrogels with E_e below ≈0.15 J m^{-3} enable cell adhesion, defining a threshold for the elastic energy of the substrate for cell adhesion. To confirm this intriguing evidence, we undertook a material's engineering approach to manipulate the linear elastic energy of agarose gels following: i) the addition of physical entanglements by a branched lactose-modified chitosan (CTL) that is not involved in hydrogel formation;[17] (ii) the addition of polystyrene beads as stress dampers (Figures S14 and S15, Supporting Information). While showing the same shear modulus, EP hydrogels supplemented with various amounts of CTL (0.5 and 1% w/V) display E_e lower than the threshold and allow for cell adhesion, although to a different extent. In the case of polystyrene beads, only the 1/400 dilution, which has

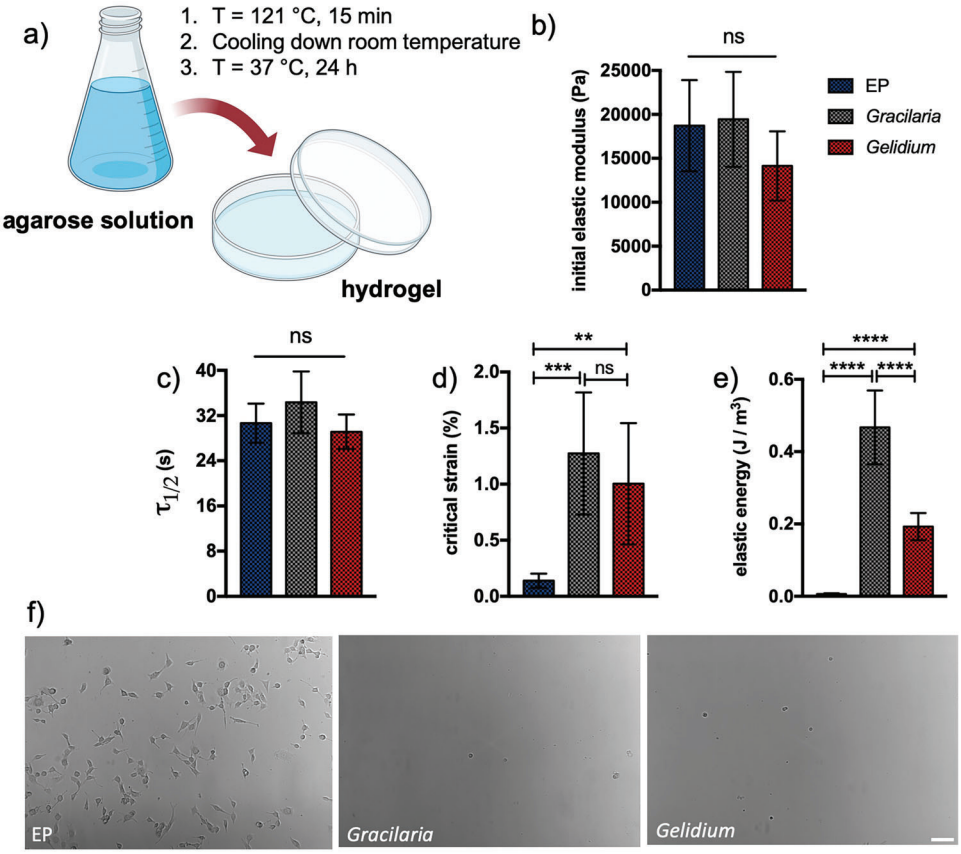

Figure 2. The chemical composition of agaroses affects the mechanical properties of the resulting hydrogels and cell adhesion. a) In this study, a 3-step temperature-assisted gelation was used to prepare agarose-based hydrogels, which included solubilization of agarose at 121 °C by autoclaving, subsequent (quenching) cooling to room temperature and a step at $T = 37$ °C for 24 h.[20] b) Initial elastic modulus from uniaxial compression measurements for hydrogels with different composition. c) Time needed to relax the stress to half of the initial value, $\tau_{1/2}$. d) Critical strain at which strain softening originates determined by oscillatory shear (rheometry). e) Linear elastic energy calculated according to Equation (1) in the main manuscript. All hydrogels were assembled in PBS buffer, pH 7.4, with constant agarose (1% w/V) amount. Data are reported as mean ± s.d., $n = 6 - 8$ hydrogels analyzed for each experimental condition. Statistics: ns, not significant; $^{**}p < 0.01$; $^{***}p < 0.001$; $^{****}p < 0.0001$ (One-way ANOVA followed by Tukey's Multiple Comparison post hoc test). f) Representative images of MG63 adhering atop hydrogels with different composition; scale bar is 200 µm.

an elastic energy lower than the threshold, allows cell adhesion. Intriguingly, the addition of fibronectin as coating, and the consequent increase in anchoring points for cells, increases the number of adherent cells only on substrates whose elastic energy is below the threshold of 0.15 J/m^3 (Figure S16, Supporting Information). However, the presence of fibronectin does not help in the case of substrates whose elastic energy is above the threshold. Taken together, these results show that there is an energy barrier in the linear elastic response of the substrate and that cells can only adhere below this threshold.

2.3. Effect of the Elastic Energy Threshold Toward Different Cell Lines

To support our findings, we next investigated the effect of elastic energy threshold toward different cell lines. For this purpose, cells were seeded on substrates with very low (EP 1% w/V), medium (EP 0.5% w/V, just below the energy threshold) and high (*Gelidium* 1% w/V, above the energy threshold) linear elastic energy. Fibroblast-like NIH-3T3 (embryo-origin), immortalized human keratinocytes HaCaT (skin-origin), human hepatoma HuH7 (liver-origin) and human hepatic stellate LX-2 (liver-origin) are selected as models and compared with the results of the MG63 cell line. All cell lines show a similar trend, with marked and limited cell adhesion on low- and medium-linear elastic energy hydrogels, respectively (**Figure 4**a,b). In contrast, the *Gelidium* substrates prevented cell adhesion under all conditions tested. Remarkably, the ratio in the number of adherent cells between medium and low linear elastic energy substrates draws an interesting scenario (Figure 4c). While NIH-3T3 is the most responsive to the change in hydrogel mechanics, there is an increase in tolerance to the elastic energy of the substrate, with HuH7 and HaCaT appearing to be the most tolerant to elastic energy modifications among the cell types used. Overall, these results confirm the role of the threshold as an energy barrier, below which the elastic energy can be tolerated differently depending on the cell type.

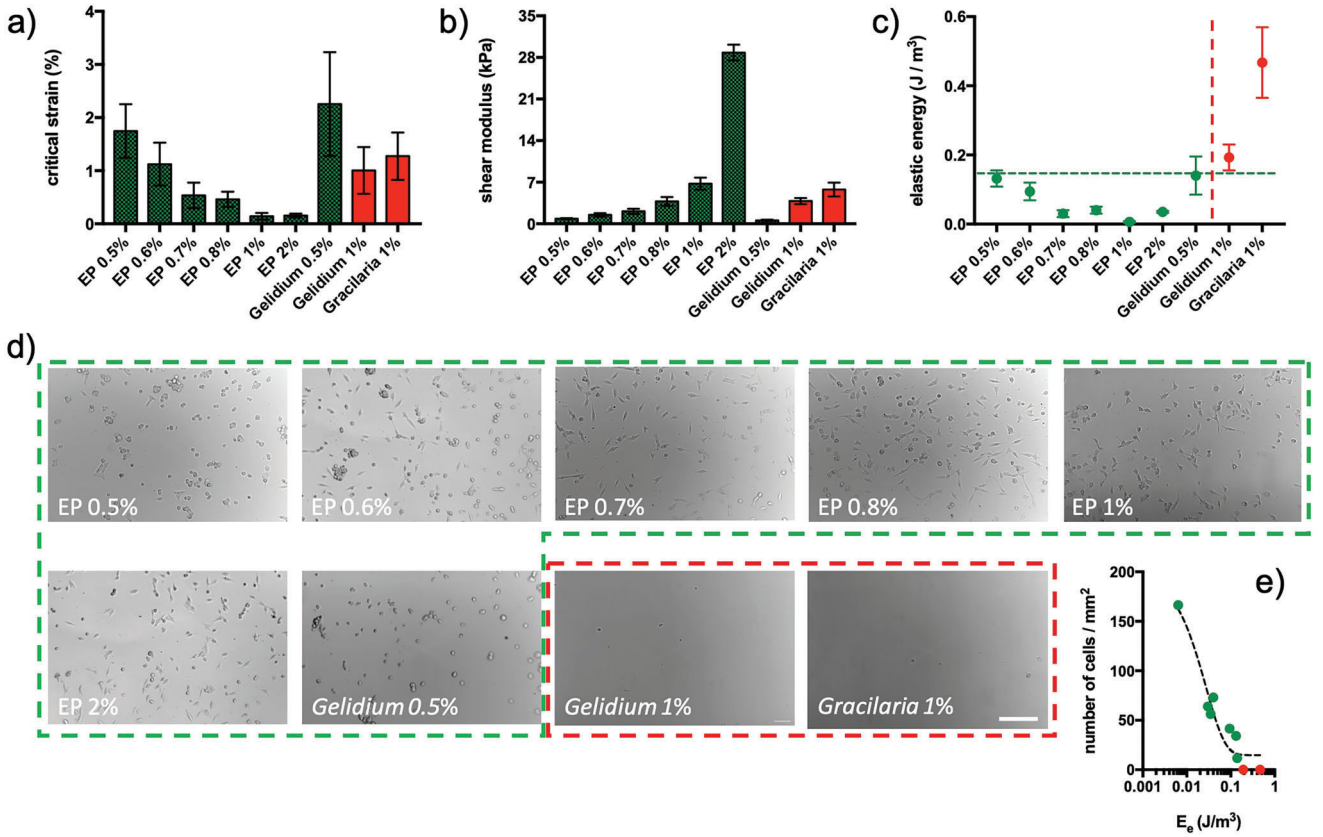

Figure 3. Adhesion of cells to viscoelastic agarose hydrogels is only permitted if the linear elastic energy of the substrate is below a threshold value. a,b) Critical strain and shear modulus for hydrogels with different composition. c) Linear elastic energy for hydrogels with different composition; the green dashed line indicates the elastic energy threshold (≈0.15 J m^{-3}), while the red dashed line delimitates the hydrogels that do not support cell adhesion. Data are reported as mean ± s.d., $n \geq 6$ hydrogels analyzed for each experimental condition. d) Representative images of MG63 adhering atop hydrogels with different composition; scale bar is 200 µm. e) Correlation plot of number of cells per mm^2 versus elastic energy of substrates used in this set of experiments; dashed black line was drawn to guide the eye.

2.4. Linear Elastic Energy Loss in the Strain-Softening Region Correlates with Cell Activities

Agarose hydrogels show plastic deformation (strain softening) when they leave the linear stress–strain regime (Appendix S4, Supporting Information). The strain softening of the hydrogel is accompanied by a reduction in the shear modulus (Appendix S5, Supporting Information). We therefore wondered whether there is a correlation between this plastic deformation of the hydrogel and the number of cells adhering to it. From the previous paragraph, we assume that the cells apply an energy in the order of 0.15 J m^{-3}, i.e., the elastic energy threshold, to the hydrogel, which is therefore deformed to a maximum strain, γ_{max}. For cell adhesion to occur E_e has to be lower than the elastic energy threshold and, consequently, $\gamma_{max} > \gamma_{crit}$. The higher the plasticity of the hydrogel, the greater the difference between γ_{max} and γ_{crit}.

On the material side, for hydrogels allowing for cell adhesion we calculated the linear elastic energy loss, E_l (Appendix S6, Supporting Information), which is the difference between the theoretical elastic energy calculated for a linear stress–strain relationship and the experimental elastic energy from γ_{crit} to γ_{max} (**Figure 5**a). E_l reflects the plastic deformation of the hydrogel: hence, the higher E_l the higher the network plasticity.

$$E_l = \int_{\gamma_{crit}}^{\gamma_{max}} \left(\left(\frac{d\sigma}{d\gamma} \right)\Big|_{\gamma=0} - \left(\frac{d\sigma}{d\gamma} \right)\Big|_{\gamma} \right) \gamma \, d\gamma \text{ with } \gamma_{max} > \gamma_{crit} \quad (2)$$

Figure 5b reports the correlation between E_l of different agarose hydrogels considered in this study and the number of adherent cells. The higher the linear elastic energy loss of the hydrogel, the higher the number of adherent cells on the agarose networks. That is, the higher the plasticity of the hydrogel, the higher the number of adherent cells. The deformation up to γ_{max} causes different outcomes for the materials. We focus on 1% w/V and 0.5% w/V hydrogels from EP agarose. While γ_{max} is higher for the latter than for the former, the variation, namely $\Delta_\gamma = \gamma_{max} - \gamma_{crit}$ shows the exact opposite trend (Figure S12, Supporting Information). It follows that γ_{max} in the 1% w/V hydrogels extends well above the linear stress–strain response, which causes a large plastic deformation. 0.5% w/V hydrogel shows the opposite trend. This reflects in the overall performance for the materials upon cyclic deformations up to γ_{max} (Figure 5c). For the 0.5% w/V

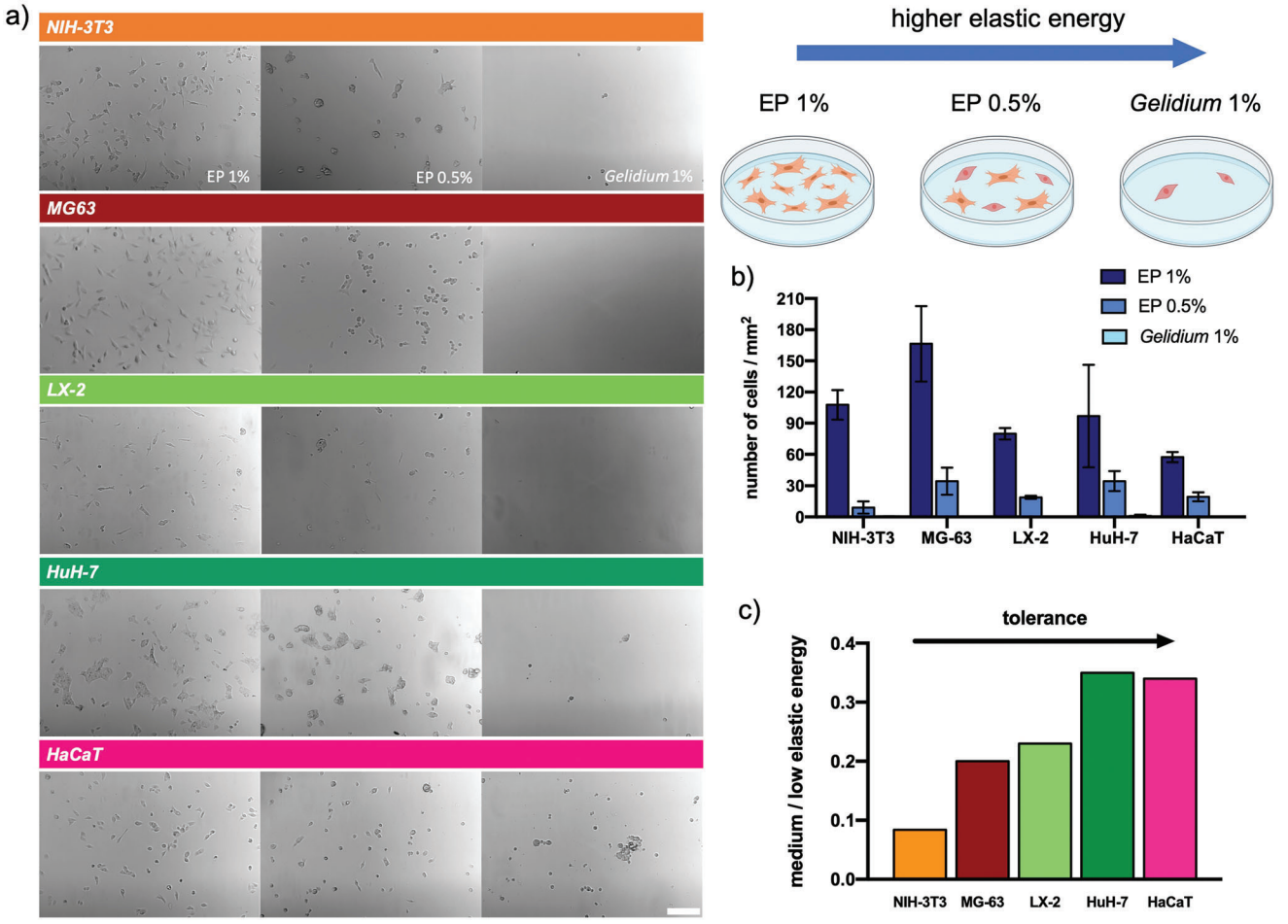

Figure 4. The elastic energy threshold is a barrier to the adhesion of cells of different origin. a) Representative images of fibroblast-like NIH-3T3, human osteosarcoma MG63, immortalized human keratinocytes HaCaT, human hepatoma HuH7 and human hepatic stellate LX-2 cells adhering atop hydrogels with different degree of linear elastic energy: low (electrophoresis, EP, 1% w/V), medium (EP 0.5% w/V) and high (*Gelidium* 1% w/V); scale bar is 200 µm. The cartoon on the right summarizes the effect of the linear elastic energy on cell adhesion. b) Number of cells per mm^2 on substrates with varying degree of linear elastic energy. Data are reported as mean ± s.d., $n \geq 6$ hydrogels analyzed for each experimental condition. c) Tolerance (ratio between the number of adherent cells on substrates with medium, EP 0.5% w/V, and low, EP 1% w/V, linear elastic energy) for cells of different origin.

hydrogel, where $\gamma_{max} \approx \gamma_{crit}$, the plastic deformation is limited and the cyclic response of the hydrogel is mainly elastic. After 10 cyclic deformations, the initial stress is decreased of a 14%, while for the first 4 cycles no variation is detected. Conversely, the effect of the cyclic loading is more substantial for the 1% w/V case, where the plastic deformation is higher since $\gamma_{max} \gg \gamma_{crit}$. In this case, the hydrogel shows a ≈85% decrease of the initial load after 10 cycles and a ≈17% already after four cycles. All in all, we expect that the higher the linear elastic energy loss in the plastic region, the greater the deformation of the substrate exerted by the cells.

2D traction force microscopy analysis monitors the force transmission of cells to 1% w/V (high linear elastic energy loss) and 0.5% w/V (low linear elastic energy loss) hydrogels of EP agarose. The force maps show a greater displacement of the embedded fluorescent beads after cell trypsinization in the 1% hydrogels than in the 0.5% counterparts, indicating greater traction stresses exerted by MG63 cells on high linear elastic energy loss substrates (Figure 5d). Confocal microscopy studies are next performed to investigate the reorganization of the substrate network (remodeling of the matrix) that takes place following the generation of cell traction forces (Figure 5e). MG63 cells plated on 1% w/V hydrogel are able to reorganize the agarose network more efficiently than cells plated on 0.5% w/V counterpart, with the largest polymer accumulations mainly at the edges of the cells. This evidence is in nice agreement with mechanotransduction studies investigating the formation of focal adhesion complexes (FAs) and visualization of actin stress fibers. On low linear elastic energy loss hydrogel (0.5% w/V), actin appears to be predominantly located in the cell periphery and organized in bundles, whereas on the high linear elastic energy loss counterpart (1% w/V), actin stress fibers are well developed and visible throughout the cytoplasm. Vinculin-rich focal adhesions indicate two distinct scenarios: the formation of greater FAs with a belt-like conformation and of punctate FAs on high and low linear elastic energy loss hydrogels, respectively. This suggests that cells plated on 1% w/V EP agarose hydrogel are in an active state of cytoskeletal reorganization triggered by full activation of the mechanotransduction

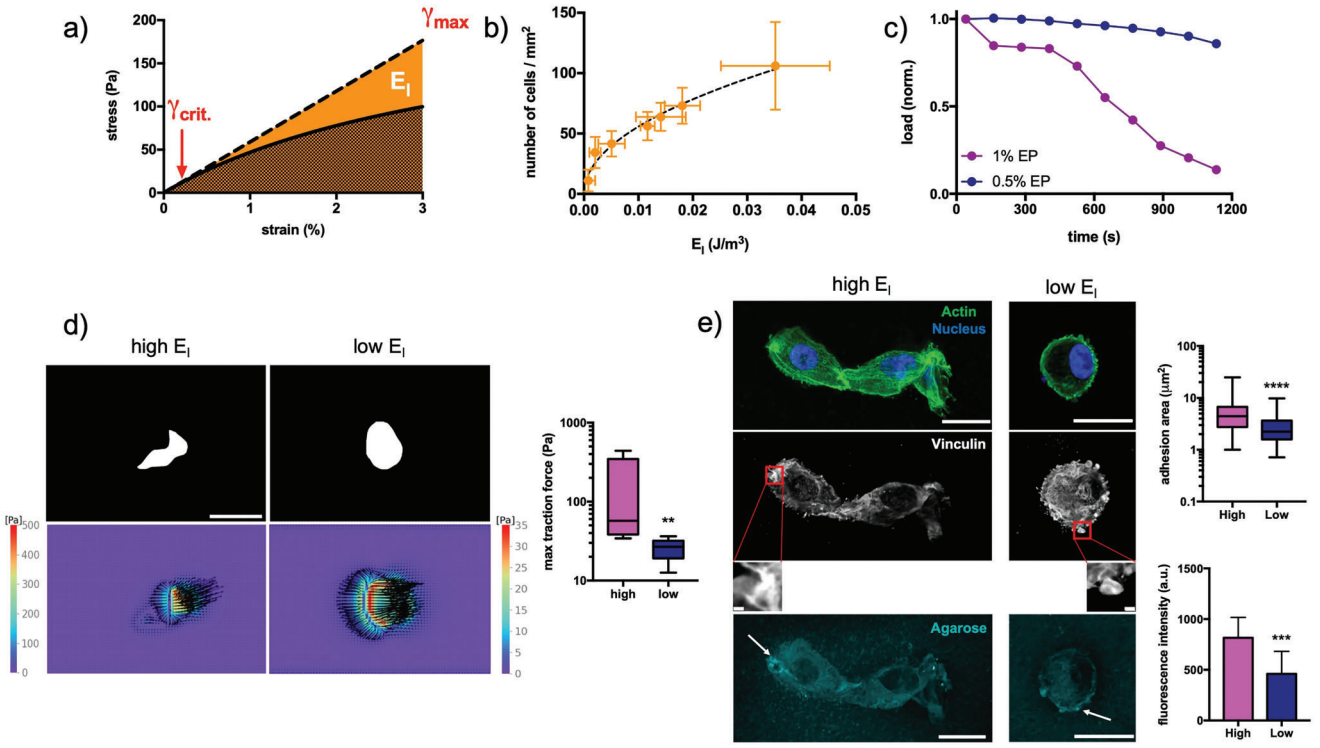

Figure 5. The linear elastic energy loss in the strain-softening region correlates with the number of cells adhering to viscoelastic substrates and their activities. a) Representative shear stress–strain curve profile of agarose-based substrates. Data are displayed up to the theoretical maximum strain identified, γ_{max} (see Appendix S5, Supporting Information, for additional details). Solid orange area in the nonlinear stress–strain region represents the linear elastic energy loss, E_l, calculated according to Equation (2) in the manuscript. b) Correlation plot of number of cells per mm^2 versus linear elastic energy loss of substrates used in this work; dashed black line was drawn to guide the eye. c) Cyclic mechanical response up to γ_{max} over time for hydrogels with different concentration of electrophoresis (EP) agarose. d) Representative images of cell mask area and traction force maps for MG63 cells cultured on EP agarose hydrogels with different degree of linear elastic energy loss ([EP agarose] = 1%, high E_l, and 0.5% w/V, low E_l); scale bar is 50 µm. Box and whiskers plot displays the maximum traction force transmitted by cells to the substrate. Data are reported as mean ± s.d., n = 4–9 cells analyzed. Statistics: $^{**}p < 0.01$ (two-tailed Mann–Whitney test). e) Immunostaining and quantification of vinculin for MG63 cells on hydrogels with different degree of linear elastic energy loss ([EP agarose] = 1%, high E_l, and 0.5% w/V, low E_l). Visualization and quantification of agarose remodeling. The fluorescence intensity stands for the agarose fluorescence intensity underneath the boundary of cell normalized by background subtraction. The arrows indicate agarose accumulation. Data are reported as mean ± s.d., n = 7–12 cells analyzed for vinculin quantification and n = 20–35 ROI images for agarose quantification. Statistics: $^{***}p < 0.001$; $^{****}p < 0.0001$ (two-tailed Mann–Whitney test). Scale bars are 20 µm, zoom-in/inset 5 µm.

cascade. Overall, these results indicate that the higher the linear elastic energy loss in the plastic strain-softening region, the stronger the transmission of forces by cells, the matrix remodeling and the transduction of biophysical cues.

3. Discussion

In the present work, agarose hydrogels with controlled mechanics are developed and used as substrate to identify a correlation between cell activities and material elastic energy. Over the last few years, cell response has been correlated predominantly to the elastic (Young's) modulus. The engagement of the molecular clutch and the related unfolding of talin was reported to take place within a specific rigidity range. This has led to propose a cell-sensitivity to the elastic modulus of the material.[23] Various authors reported that substrate elasticity affects cell adhesion, spreading and migration,[24] as well as proliferation and apoptosis.[25,26] However, recognizing that natural ECM has viscoelastic properties has led to a novel interpretation on the role of substrate mechanics, addressing both the elastic and viscous response of the microenvironment as a key aspect to understand cell behavior.[27] The role of viscoelastic and plastic properties is nowadays the subject of intense research,[2–10,28] and the concept of dissipation and storage of energy by viscoelastic substrates regulating cell activities has been put forward quite recently. Mechanistically, natural tissues and extracellular matrices can dissipate forces under stress, which depends on the nature of the cross-links, slip and slide phenomena, the release of polymeric entanglements, and protein unfolding.[1,15,17,29–33] Furthermore, under tension or compression, dissipation occurs due to the flow of water into or out of the network within the extracellular matrix resulting from volume changes (poroelasticity).[1]

In the present work we start comparing three agarose samples characterized by a different methylation pattern. All the three samples show initial elastic modulus > 15 kPa (Figure 2b), thus above the threshold value required to trigger force transduction.[12] In addition, all three samples show similar stress relaxation time (Figure 2c), namely in the range from 30 to 40 s, well within the range reported to be essential for cell spreading, proliferation, and differentiation.[4] Nevertheless, while

hydrogels from EP agarose are permissive for cell adhesion, no cell adhesion is shown by agarose hydrogels from *Gelidium* or *Gracilaria*. These considerations imply that, in addition to stiffness and viscoelasticity, the amount of sole energy stored by the substrate, in terms of linear elastic energy, is also crucial for cell adhesion in 2D cultures.

Focusing on the hydrogels from the three agarose samples (Figure 3a–c), the different pattern of methylation causes a substantial modification in the critical strain that marks the onset of strain-softening under oscillatory shear conditions. Specifically, the methylation at A2 and G4 acts extending the linear stress–strain relationship of the hydrogel, with the latter being more effective than the former. This reflects into a substantial difference in the linear elastic energy needed to exit from linear stress-strain regime and, in turn, in cell adhesion. These results seem to point to an elastic energy threshold above which cells do not adhere. To test this hypothesis, we have used several agarose hydrogel systems, varying the polysaccharide concentration to tune the shear modulus, the critical strain and the linear elastic energy. No correlation is found for cell adhesion on the shear modulus or critical strain for the different hydrogels tested. Our results indicate that a trend exists when the linear elastic energy is considered (Figure 3d,e). All hydrogels with an elastic energy of less than $\approx$0.15 J m^{-3} allow cell adhesion, while substrates exceeding this threshold are no longer permissive.

It is known that the response to substrates is cell-specific and could be correlated with the mechanical properties of the environment naturally sensed by the different cells.[34,35] Recently myoblasts have been reported to self-organize in isotropic and highly deformable gelatin hydrogels with a Young's modulus $\leq$ 6 kPa, although the deformation of the substrate was evaluated on the basis of the Young's modulus and no analyses on viscoelasticity were conducted.[36] Interestingly, here we demonstrate that all the cell types used in this study show an energy-sensing ability with adaptable tolerance (Figure 4), likely acting via a pushing-pulling mechanism toward the matrix to gauge the mechanical properties of the substrate.[37]

It has been demonstrated that cells can remodel the matrix and reorganize the surrounding environment by means of the sole mechanical forces, managing to re-orientate and align fibers in an irreversible way.[29] In our case, the permanent deformation upon cyclic loading is correlated with E_l, being higher for the substrate showing a high linear elastic energy loss (Figure 5c). The energy threshold is here interpreted as the total energy transferred to the substrate, which causes a plastic deformation, detected as E_l, when higher than the linear elastic energy, E_e (**Figure 6**, cartoon). In this context, we tried to correlate the mechanical model with the mechanotransmission of cells on the same substrates. Strikingly, the cells on the 1% w/V EP substrate transmit more forces and are able to efficiently remodel the polymer matrix beneath their surface (Figure 5d). Conversely, the cells on the 0.5% EP counterpart seemed less inclined to remodel the substrate. This body of evidence indicates that in the case of 1% w/V EP hydrogel (high E_l, i.e., high plasticity) cells generate enough traction forces to remodel the polymeric structure of the substrate and elicit the focal adhesion assembly. This is confirmed by the large, belt-like focal adhesions that are formed (Figure 5e). On the opposite, cells transmit lower traction forces toward 0.5% w/V EP hydrogel (low E_l, i.e., low plasticity) through small, dot-like focal adhesions, which cause less pronounced agarose concentration underneath the cell body.

Taking the results of this work together, we propose that the cells sense a linear elastic energy feedback to adhere to the substrate. When the elastic energy of the substrates exceeds a threshold—in our set of viscoelastic substrates this is $\approx$0.15 J m^{-3}—cells can no longer adhere. In contrast, when the elastic energy of the substrate is set lower than 0.15 J m^{-3}, cells can adhere. Additional and more complex considerations must be made when taking into account the nonlinear stress–strain region, which in our case is manifested by strain-softening behavior under oscillatory shear stress. We find a good correlation between the number of cells attached to the substrate and the amount of theoretical linear elastic energy loss calculated by a mathematical approach (Figure 5). How this translates in vitro is currently unknown, but it is likely that the elastic energy loss could act as substrate plasticity, which is known to influence cell activities. In this work, for example, we have demonstrated that the higher E_l is, the higher the remodeling of the matrix and the mechanotransduction processes are (Figure 6, cartoon). More knowledge needs to be gained to shed light on this intriguing topic.

Accurate information of the relationship between cell adhesion and the energy threshold of viscoelastic substrates is an important aspect of developing reliable ex vivo models of human tissues that mimic both normal and pathological conditions. In this regard, the data obtained in this work can, for example, help to develop an effective in vitro model for culturing hepatic stellate cells (HSCs, represented here by the LX2 cell line). HSCs, which exhibit characteristics of fibroblasts, are localized in the liver where they can undergo activation (proliferation/migration) due to various pathological stimuli (viral infection, toxic substances).[38] Upon activation LX2 produce an aberrant extracellular matrix, possibly altering the energy threshold compared to the normal liver. This in turn leads to the formation of scar tissue that gradually depletes liver functions. Therefore, in order to study in vitro drugs that counteract the activation of HSCs, it is necessary to generate substrates that reflect the altered elastic energy both in the linear and nonlinear stress–strain region.

4. Experimental Section

Agarose Sources and Analyses: Native agar from *Gracilaria* was kindly provided by Java Biocolloid (Trieste, Italy). Native agar from *Gelidium* (Oxoid Agar Bacteriological) was purchased from Thermofisher Scientific. Agarose sample for Electrophoresys (code EMR920500) was purchased from (Euroclone, Italy). The determination of the gelling temperature was determined by hard-shaking method. Briefly, 25 mL of 1.5% w/V agarose sample were poured in a graduated cylinder, following solubilization under reflux for 15 min and sterilization by autoclave. An analogical thermometer was inserted and the cylinder shaken vigorously for 10 s. The movement of air bubbles in the sample was checked. The cylinder shaking was repeated while the temperature was decreasing until the air bubbles remained still. The temperature indicated by the thermometer indicated as the gelling temperature. Rotational viscosity: 250 mL of 1.5% w/V agarose sample were poured into a beaker, following solubilization under reflux for 15 min and sterilization by autoclave. Rotational viscosity was measured at different temperatures with a Digital Viscometer (Biobase, Model BDV-1S). Rotor 3 was used and the speed of the viscometer was set to 30 rpm. Ash determination: ceramic crucibles were placed in a muffle (Electric Furnace, Model SX2-2.5-10) at $T = 550$ °C overnight. The following day, the crucibles

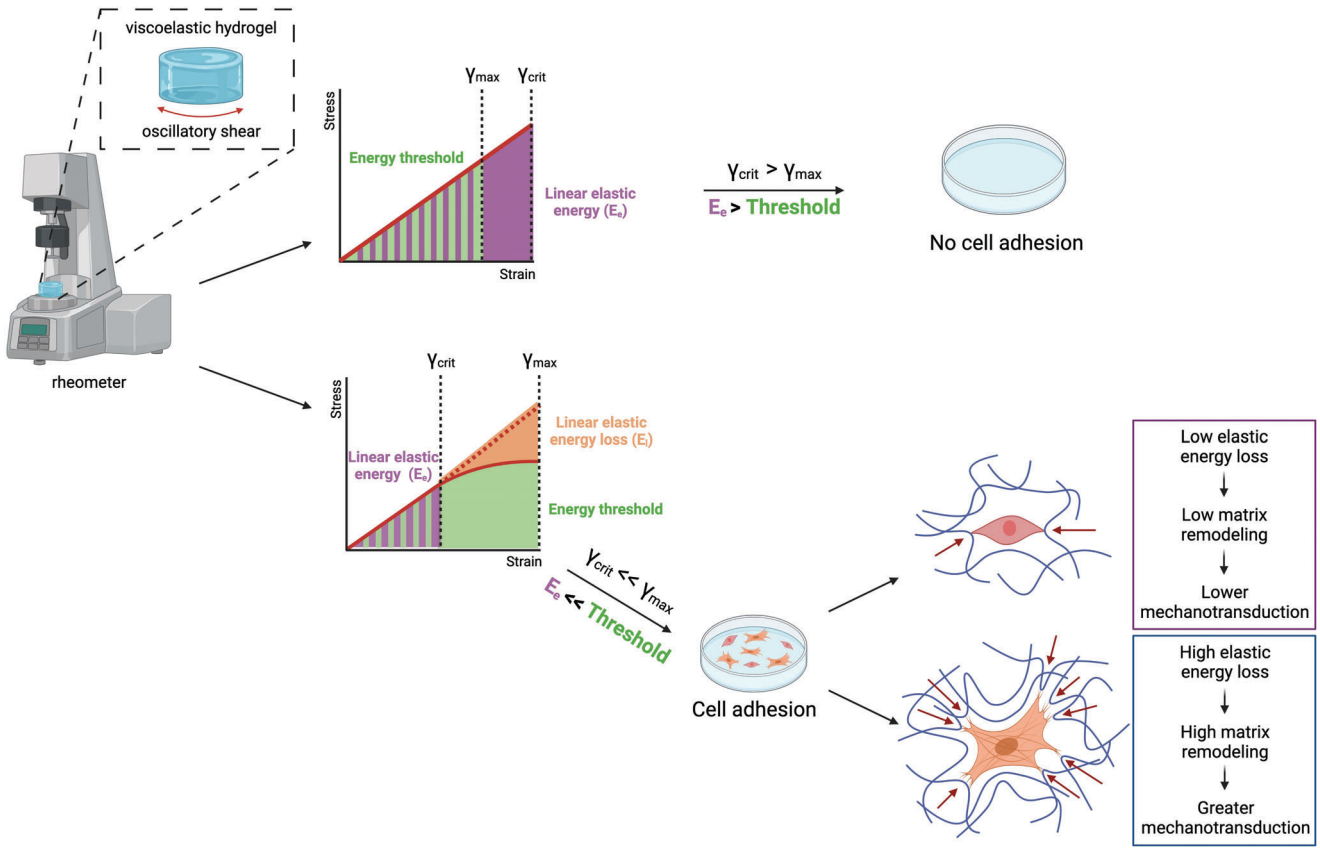

Figure 6. Cell activities on viscoelastic substrates show an elastic energy threshold and correlate with the linear elastic energy loss in the strain-softening region. Schematic cartoon summarizing what was identified in this study. Agarose-based viscoelastic hydrogels exhibit a linear stress–strain response followed by a softening behavior upon oscillatory shear stimulation. By varying the physical and chemical properties of the hydrogels, we finely modulated the elastic energy required to exit the linear stress–strain regime. The linear elastic energy sets a threshold (≈0.15 J m^{-3}) for cell adhesion: below the threshold, cells can attach to the substrate with varying degrees of activities, while above the threshold this is no longer possible. Importantly, we found a correlation between the calculated linear elastic energy loss (E_l) in the strain softening (plastic) region and the number of cells adhering to the substrate. When E_l is set high, cells with well-established vinculin-rich anchoring points can spread while remodeling the underlying matrix by greater traction forces. On the other hand, if E_l is set low, cells are less inclined to spread and remodel the substrate network.

were moved to a desiccator for 5 h and their weight recorded (cup initial weight). The moisture of each agarose sample was measured with a Moisture Analyzer thermobalance (Chanzhon Xingyum Electronic, Equipment Co. Ltd). Subsequently, 5 g of each agarose sample was weighed inside the crucible (Sample powder Initial weight) and processed by combustion. When the sample was completely burned, the crucibles were placed in the muffle at 550 °C overnight. The following day, crucibles were placed in a desiccator for 5 h and their weight recorded (cup final weight). The content of ashes was calculated as follows:

$$\%\ \text{Ashes} = \frac{\text{cup final weight} - \text{cup initial weight}}{\text{sample powder initial weight} \times \frac{100 - \text{moisture}}{100}} \times 100 \qquad (3)$$

The chemical composition of agaroses was determined by ^{1}H-NMR measurements through a Varian VNMRS-500 (11.74 T) and a Varian 400-MR NMR spectrometer (9.4 T), operating for proton at 500 and 400 MHz, respectively. The ^{13}C and 2D spectra were recorded exclusively on the Varian VNMRS-500 spectrometer, which is equipped with a 5 mm indirect detection broadband gradient probe. The spectra were recorded at T = 80 °C from D_2O solutions, previously kept at 90 °C for 30 min to attain the complete dissolution of the gels. Chemical shifts are referred to 3-(trimethylsilyl)propanesulfonate. For proton 256 scans were acquired over 16 K complex points employing a spectral width of 5980.9 Hz over 16 K complex points, on the 500 MHz NMR spectrometer. For carbon 8000 scans were accumulated using a spectral width of 31 250 Hz over 32 K complex point. The multiplicity-edited HSQC 2D spectra were carried out by the gradient selected sequence with adiabatic pulses HSCQAD, encoded in the Vnmrj software, accumulating 32 scans over 897 complex points for each of the 400 t1 increments. The spectral widths were 5980.9 and 25 117.7 Hz for ^{1}H and ^{13}C, respectively. The ^{13}C resonances were assigned according to the literature.[39,40]

Synthesis of Atto Rho101 NHS Ester-Labeled Agarose: An amount of 300 mg of agarose was dispersed in 15 mL of deionized water and resulting mixture stirred at ≈95 °C for 15 min to promote agarose solubilization. Then, reaction temperature was cooled down at 60 °C and 125 µL of Atto Rho101 NHS ester (Sigma, USA) dissolved in DMSO at 2 mg mL^{-1} were added to the solution. The reaction mixture was stirred for 30 min and in dark conditions. The mixture was then poured into a Petri dish and let to gel at room temperature. Next, labeled-agarose gel was cut into small pieces, extensively washed in deionized water, frozen overnight at −20 °C and thawed the day after. Freeze–thaw steps were repeated thrice to eliminate most of solvent. The labeled-agarose was finally vacuum-dried at 60 °C and milled in a mortar.

Hydrogels Preparation: Agarose powders from different sources (final concentration 0.5–2% w/V) were added to 1× PBS buffer, pH 7.4. The resulting mixtures were autoclaved (T = 121 °C, 15 min) and placed in cylindrical supports before cooling at room temperature. The hydrogels were

finally incubated 24 h at 37 °C under water-saturated conditions to prevent evaporation of the solvent.

Mechanical Characterization: Rheological characterization of hydrogel disks (20 mm in diameter, 2 – 2.5 mm thick, PBS buffer) was performed by means of a controlled stress rheometer HAAKE MARS III operating at $T = 37$ °C using a shagreened plate-plate apparatus ("HPP20 *profiliert*": diameter = 20 mm) as the measuring device. To avoid water evaporation from hydrogels, measurements were performed in a water-saturated environment formed by using a glass bell (solvent trap) containing a wet cloth. In addition, to prevent both wall-slippage and excessive hydrogel squeezing, the gap between plates was adjusted by executing a series of short stress sweep tests ($\nu = 1$ Hz; stress range 1–5 Pa) until a constant G' was reached. The linear viscoelastic range was determined by means of stress sweep tests consisting in measuring the elastic (G') and viscous (G'') moduli variation with increasing shear stress ($1\ \text{Pa} < \tau < 1000\ \text{Pa}$) at a frequency $\nu = 1$ Hz (hence with $\omega = 2\pi\nu = 6.28\ \text{rad s}^{-1}$). The mechanical spectra (frequency sweep tests) were recorded by measuring the dependence of the elastic (G') and viscous (G'') moduli on pulsation frequency at constant shear stress $\tau = 5$ Pa (well within the linear viscoelastic range).

Uniaxial compression of hydrogel disks (16 mm in diameter, 17 mm thick, PBS buffer) was performed by means of a universal testing machine (Mecmesin Multitest 2.5-i) equipped with a 100 N load cell. A compression speed of 1 mm min^{-1} was applied to determine initial elastic modulus in the strain range 1–3%. Stress–relaxation tests have been conducted by applying a constant strain of 15% and recording the stress required to maintain constant the strain for 600 s; a speed of 10 mm min^{-1} was used in the stress loading phase. The time needed to relax the stress to half of the initial value, $\tau_{1/2}$, was considered as parameter to compare hydrogels with different composition.

Synthesis of FITC-Labeled BSA: A total of 400 mg of bovine serum albumin (BSA, Sigma) were dissolved in 10 mL of $NaHCO_3$ 30×10^{-3} M. Then, 500 µL of a Fluorescein-isothiocyanate (FITC, Sigma) solution (2 mg mL^{-1} in pure ethanol) was added to the BSA solution. The reaction mixture was stirred for 24 h at room temperature and under dark conditions. The mixture was then dialyzed at 4 °C against $NaHCO_3$ 30×10^{-3} M (two shifts, V = 500 mL) and deionized water (three shifts, $V = 1$ L). All steps were carried out under dark conditions. Finally, the solution was freeze-dried.

Evaluation of BSA Absorption on the Hydrogels Surface: 1% w/V hydrogels of agarose from different origin were incubated O/N at 37 °C with 1.6 mL of FITC-labeled BSA (0.5 w/V dispersed in PBS). The next day, the BSA solution was discarded and the hydrogels were washed extensively with PBS to remove nonadherent BSA and punched to obtain 6 mm diameter discs. They were then placed on a coverslip and analyzed by confocal microscopy using a Plan Fluor 20× objective. A series of images were saved at 266 × 266 µm with 4 µm *z*-resolution step size. The images were acquired with identical acquisition settings to allow comparison of fluorescence intensities between the analyzed samples and were processed with Fiji-ImageJ. Fluorescence intensity was quantified within 8 µm depth from the hydrogel surface by measuring the intensity of 8–10 different 10 × 10 µm fields using the ImageJ ROI manager tool.

Cell Culture: Human osteosarcoma MG63 (ATCC CRL-1427), fibroblast-like NIH-3T3 (ATCC CRL-1658), immortalized human keratinocytes HaCaT, human hepatoma HuH7,[41] and human hepatic stellate LX-2 were cultured in Dulbecco's modified Eagle's Medium High glucose with 0.584 g L^{-1} L-glutamine and 0.11 g L^{-1} sodium pyruvate (EuroClone, Italy), supplemented with 10% heat-inactivated fetal bovine serum (Cat. no. ECS5000L; Lot. No. EUS00K1, Euroclone, Italy) and 1% penicillin/streptomycin (EuroClone, Italy), in a humidified atmosphere of 5% CO_2 at 37 °C.

Plating of Cells Atop Hydrogels (Substrates): After autoclaving, the agarose mixtures were transferred to a water bath preheated to $T = 60$ °C and left for 10 min. For the experiments in the presence of lactose-modified chitosan (CTL), CTL solutions were prepared by dissolving the CTL powder in PBS buffer to obtain concentrations of 0.5% to 1.5% w/V. Agarose was then added to the solutions and the mixtures were subjected to the same temperature cycle. Additional experiments were performed in the presence of carboxylate-modified FluoSpheres (dilution 1:100 to 1:400, 0.2 µm, Invitrogen) in the agarose mixture. After the temperature cycle, 400 µL of the mixtures were distributed into 24-well plates and allowed to rest for 30 min at room temperature to promote gelation. Finally, the substrates were incubated 24 h at 37 °C in water-saturated conditions. For experiments with fibronectin coating, the substrates were additionally incubated overnight at 4 °C with 300 µL fibronectin (Sigma) dispersed in PBS. The next day, the PBS was discarded and the substrates were washed with cold PBS. Cells were trypsinized and plated out at a density of 30 000 cells per well in 1.6 mL cell culture medium/well supplemented with fetal bovine serum, giving a final V_{PBS}/V_{medium} ratio of 20:80 v/v. The cells were incubated O/N in a humidified atmosphere with 5% CO_2 at 37 °C.

Assessment of Cell Adhesion: After overnight incubation, cell culture medium was discarded and substrates washed extensively with PBS in order to remove nonadherent cells. Then, 300 µL per well of PBS were added and the number of adherent cells mm^{-2} was quantified by Fiji-ImageJ software (multipoint tool) from images acquired through a Nikon Ti Eclipse inverted bright-field microscope equipped with a Plan Fluor 10× objective.

Cell Immunostaining and Image Analysis: Cells were plated atop 0.5% and 1% w/V EP agarose hydrogel containing Atto Rho101 NHS ester-labeled agarose (20% w/w). After overnight incubation, cell culture medium was discarded and substrates washed extensively with PBS in order to remove nonadherent cells. Then, substrates were punched into small disks (9 mm in diameter, 2.5 mm thick) and moved in clean 48-well plate. Cells were fixed with formaldehyde 4% V/V (Sigma) in PBS for 30 min at room temperature. Then, substrates were washed 5× with PBS and permeabilized with Triton 0.2% V/V (Sigma) in PBS for 15 min at room temperature. Next, substrates were washed with PBS and incubated with BSA 4% w/V (Sigma) + Normal Goat Serum 5% V/V (Sigma) in PBS for 1 h at 37 °C. The blocking solution was then removed and the samples washed with PBS. The following primary antibody was used for immunostaining: vinculin antibody (dilution 1:200 or 5 µg mL^{-1}, V9264, Sigma). Primary antibody was diluted in blocking mixture. Incubation proceeded overnight at 4 °C. Then, cells were washed and incubated with secondary antibody mouse IgGk light chain diluted in blocking solution (dilution 1:250 or 1.6 µg mL^{-1}, sc-516179, Santa Cruz) for 2 h at room temperature. For the visualization of F-actin filaments and nuclei, cells were counterstained with Phalloidin Fluorescein Isothiocyanate Labeled (P5282, Sigma, 1 µg mL^{-1} in PBS) and Hoechst (33 258, Invitrogen, 5 µg mL^{-1} in PBS), respectively. Finally, substrates were washed once and stored in PBS. Images from immunofluorescence and cellular staining experiments were acquired using a Nikon C1si confocal microscope (Nikon, Tokyo, Japan), containing 488 nm (argon), 408 nm and 561 nm (diode) lasers. Light was delivered to the sample with an 80/20 reflector. The system was operated with a pinhole size of one Airy disk. Electronic zoom was kept at minimum values for measurements to reduce potential bleaching. For the different fields collected we used 40x Plan Apo objectives, saving series of optical images with 1 µm *z*-resolution step size. Images in various conditions were captured under identical acquisition settings in order to allow comparison of fluorescent intensity and were processed for maximum z-projection by using Fiji-ImageJ (NIH, Bethesda, USA). The staining quantification was performed and analyzed by the ImageJ tool ROI manager.

Traction Force Microscopy and Matrix Remodeling: After overnight incubation, substrate disks assembled with carboxylate-modified FluoSpheres (0.2 µm, red 580/605, Invitrogen, dilution 1:700) were placed in an inverted microscope equipped with a 40x objective and the cells were trypsinized. The images were acquired through a Nikon Ti Eclipse inverted bright-field microscope at different time steps in order to monitor the evolution for a time interval of 30 min after the addition of trypsin. Image pixel size was $0.073 \times 0.073\ \mu\text{m}^2$ and several layers of 3 µm were acquired. The brightfield and the red-fluorescence images are acquired for each time step. Traction force analyses were performed by means of pyTFM software package.[42] Images were first pre-processed to compensate for noise and BM3D[43] was found to be an effective denoising filter. A 2× digital re-bin was also performed. After that, images were co-registered via rigid registration in order to compensate for stage drifts between first and last time steps. The deformation field using particle image velocimetry (PIV) was computed by following the recommended window size (about 6 times the size of the bead) and overlap (no less than half of the window size). Traction force and stress maps were then derived assuming a Young's modulus of 18 kPa for

the 1% w/V hydrogel and 2.5 kPa for 0.5% w/V counterpart. Poisson's ratio was set to 0.5 for both cases. Thanks to the corresponding brightfield image, the region-of-interest covered by the cell was segmented in the red-fluorescence images, thus to extract numerical results only in the significant area. Separated color bars are used to better assess the local stresses and vector arrows are also added as suggested by the pyTFM software in order to infer the direction of the forces. Maximum force and stress exerted by cells were assessed. To measure the matrix remodeling caused by cell traction forces, osteosarcoma MG63 cells were plated atop Atto Rho101 NHS ester-labeled agarose substrates, immunostained as previously described, and visualized by means of confocal microscopy. Images were then analyzed using Fiji-ImageJ software to extrapolate the fluorescence intensity of agarose in different ROI directly underneath the cell boundary. The values were then normalized by background subtraction, where the background was the fluorescence intensity of a ROI far from the cell.

Statistical Analysis and Software: Statistical comparisons and graphical elaborations were carried out using GraphPad Prism software. A one-way ANOVA (analysis of variance) was performed, followed by a Tukey post hoc test to assess differences between the different groups. An unpaired Mann–Whitney two-tailed *t*-test was performed to assess differences between two groups. Differences were considered significant if the *p*-value was less than 0.05. The cartoons have been created with BioRender.com.

Supporting Information

Supporting Information is available from the Wiley Online Library or from the author.

Acknowledgements

Confocal images reported in this article were generated in the Light Microscopy Imaging Center of the University of Trieste at the Life Sciences Department, funded as detailed at www.units.it/confocal. This study was supported by the grant D40-microgrants23_SACCO. G.G. wishes to thank the Italian Ministry of Foreign Affairs and International Cooperation (project VN21GR01). The authors wish to thank Prof. Ralf Weiskirchen (Institute of Molecular Pathobiochemistry, Experimental Gene Therapy and Clinical Chemistry, RWTH University Hospital Aachen, Aachen, Germany) for providing LX2 cells.

Conflict of Interest

The authors declare no conflict of interest.

Author Contributions

P.S. and I.D. conceptualized the study. F.P., P.S., E.M., G.B., F.B., F.A., G.G., M.G., and I.D. worked on methodology. F.P., G.B., and F.B. contributed in software. F.P., G.B., F.A. investigated the work. F.P., P.S., E.M., F.B., F.A., M.G., I.D. worked on data curation. P.S., I.D. supervised the work. F.P., P.S., and I.D. wrote the manuscript.

Data Availability Statement

The data that support the findings of this study are available from the corresponding author upon reasonable request.

Keywords

cell activity, elastic energy threshold, mechanotransduction, mechanotransmission, viscoelastic substrates

Received: June 26, 2023
Revised: August 18, 2023
Published online: September 13, 2023

[1] O. Chaudhuri, J. Cooper-White, P. A. Janmey, D. J. Mooney, V. B. Shenoy, *Nature.* **2020**, *584*, 535.
[2] N. Török, S. Weiguo, F. S. Kolade, A. Stanford, Y. Li, S. Md, F. Rabbi, L. Vancza, S. Dongning, C. Stanford, K. Kunimoto, S. Gergely, M. Stanford, Y. Li, J. Tao, S. Monga, G. Charville, R. Wells, R. Dhanasekaran, T. Kim, O. Chaudhuri, *Res. Square* **2022**.
[3] H. Lee, L. Gu, D. J. Mooney, M. E. Levenston, O. Chaudhuri, *Nat. Mater.* **2017**, *16*, 1243.
[4] O. Chaudhuri, L. Gu, D. Klumpers, M. Darnell, S. A. Bencherif, J. C. Weaver, N. Huebsch, H. Lee, E. Lippens, G. N. Duda, D. J. Mooney, *Nat. Mater.* **2016**, *15*, 326.
[5] K. Adebowale, Z. Gong, J. C. Hou, K. M. Wisdom, D. Garbett, H. Lee, S. Nam, T. Meyer, D. J. Odde, V. B. Shenoy, O. Chaudhuri, *Nat. Mater.* **2021**, *20*, 1290.
[6] K. H. Vining, A. Stafford, D. J. Mooney, *Biomaterials* **2019**, *188*, 187.
[7] A. Bauer, L. Gu, B. Kwee, W. A. Li, M. Dellacherie, A. D. Celiz, D. J. Mooney, *Acta Biomater.* **2017**, *62*, 82.
[8] I. A. Marozas, K. S. Anseth, J. J. Cooper-White, *Biomaterials* **2019**, *223*, 119430.
[9] I. A. Marozas, J. J. Cooper-White, K. S. Anseth, *New J. Phys.* **2019**, *21*, 045004.
[10] E. E. Charrier, K. Pogoda, R. G. Wells, P. A. Janmey, *Nat. Commun.* **2018**, *9*, 449.
[11] C. E. Chan, D. J. Odde, *Science* **2008**, *322*, 1687.
[12] A. Elosegui-Artola, R. Oria, Y. Chen, A. Kosmalska, C. Pérez-González, N. Castro, C. Zhu, X. Trepat, P. Roca-Cusachs, *Nat. Cell Biol.* **2016**, *18*, 540.
[13] M. Bennett, M. Cantini, J. Reboud, J. M. Cooper, P. Roca-Cusachs, M. Salmeron-Sanchez, *Proc. Natl. Acad. Sci. U. S. A.* **2018**, *115*, 1192.
[14] Z. Gong, S. E. Szczesny, S. R. Caliari, E. E. Charrier, O. Chaudhuri, X. Cao, Y. Lin, R. L. Mauck, P. A. Janmey, J. A. Burdick, V. B. Shenoy, *Proc. Natl. Acad. Sci. U. S. A.* **2018**, *115*, E2686.
[15] C. Huerta-López, A. Clemente-Manteca, D. Velázquez-Carreras, F. M. Espinosa, J. G. Sanchez, P. Sáez, Á. Martínez-del-Pozo, S. Martín-Colomo, A. Rodríguez-Blanco, R. Esteban-, F. M. Martín-Zamora, L. I. Gutierrez-Rus, R. García, A. Elosegui-Artola, M. A. del Pozo, E. Herrero-Galán, G. R. Plaza, J. Alegre-Cebollada, *bioRxiv* **2022**.
[16] P. Sacco, G. Baj, F. Asaro, E. Marsich, I. Donati, *Adv. Funct. Mater.* **2020**, *30*, 2001977.
[17] P. Sacco, F. Piazza, C. Pizzolitto, G. Baj, F. Brun, E. Marsich, I. Donati, P. Sacco, F. Piazza, G. Baj, I. Donati, C. Pizzolitto, E. Marsich, F. Brun, *Adv. Funct. Mater.* **2022**, *32*, 2200309.
[18] A. Travan, S. Fiorentino, M. Grassi, M. Borgogna, E. Marsich, S. Paoletti, I. Donati, *Int. J. Biol. Macromol.* **2015**, *78*, 363.
[19] D. Calciu-Rusu, E. Rothfuss, J. Eckelt, T. Haase, H. B. Dick, B. A. Wolf, *Biomacromolecules* **2007**, *8*, 1287.
[20] F. Piazza, P. Parisse, J. Passerino, E. Marsich, L. Bersanini, D. Porrelli, G. Baj, I. Donati, P. Sacco, *Adv. Healthcare Mater.* **2023**, 2300973.
[21] Y. Freile-Pelegrín, E. Murano, *Bioresour. Technol.* **2005**, *96*, 295.
[22] E. Murano, R. Toffanin, F. Zanetti, S. H. Knutsen, S. Paoletti, R. Rizzo, *Carbohydr. Polym.* **1992**, *18*, 171.
[23] V. Swaminathan, M. Gloerich, *Curr. Opin. Cell Biol.* **2021**, *72*, 72.
[24] R. J. Pelham Jr, Y. l. Wang, *Proc. Natl. Acad. Sci. U. S. A.* **1997**, *94*, 13661.
[25] D. E. Discher, P. Janmey, Y.-L. Wang, *Science* **2005**, *310*, 1139.
[26] V. Vogel, M. Sheetz, *Nat. Rev. Mol. Cell Biol.* **2006**, *7*, 265.
[27] M. Cantini, H. Donnelly, M. J. Dalby, M. Salmeron-Sanchez, *Adv. Healthcare Mater.* **2020**, *9*, 1901259.

[28] K. M. Wisdom, K. Adebowale, J. Chang, J. Y. Lee, S. Nam, R. Desai, N. S. Rossen, M. Rafat, R. B. West, L. Hodgson, O. Chaudhuri, *Nat. Commun.* **2018**, *9*, 4144.
[29] S. Nam, J. Lee, D. G. Brownfield, O. Chaudhuri, *Biophys. J.* **2016**, *111*, 2296.
[30] F. H. Silver, J. W. Freeman, G. P. Seehra, *J. Biomech.* **2003**, *36*, 1529.
[31] W. Yang, V. R. Sherman, B. Gludovatz, E. Schaible, P. Stewart, R. O. Ritchie, M. A. Meyers, *Nat. Commun.* **2015**, *6*, 6649.
[32] X. Zhao, *Soft Matter* **2014**, *10*, 672.
[33] E. P. Debenedictis, S. Keten, *Soft Matter* **2019**, *15*, 1243.
[34] P. C. Georges, P. A. Janmey, *J. Appl. Physiol.* **2005**, *98*, 1547.
[35] A. J. Engler, M. A. Griffin, S. Sen, C. G. Bönnemann, H. L. Sweeney, D. E. Discher, *J. Cell Biol.* **2004**, *166*, 877.
[36] J. H. Jensen, S. D. Cakal, J. Li, C. J. Pless, C. Radeke, M. L. Jepsen, T. E. Jensen, M. Dufva, J. U. Lind, *Sci. Rep.* **2020**, *10*, 13305.
[37] B. Trappmann, J. E. Gautrot, J. T. Connelly, D. G. T. Strange, Y. Li, M. L. Oyen, M. A. Cohen Stuart, H. Boehm, B. Li, V. Vogel, J. P. Spatz, F. M. Watt, W. T. S. Huck, *Nat. Mater.* **2012**, *11*, 642.
[38] P. Acharya, K. Chouhan, S. Weiskirchen, R. Weiskirchen, *Front. Pharmacol.* **2021**, *12*.
[39] I. J. Miller, J. W. Blunt, *Bot. Mar.* **2000**, *43*, 263.
[40] Y. Gu, K. L. Cheong, H. Du, *Chem. Cent. J.* **2017**, *11*, 104.
[41] H. Nakabayashi, K. Taketa, K. Miyano, T. Yamane, J. Sato, *Cancer Res.* **1982**, *42*, 3858.
[42] A. Bauer, M. Prechová, L. Fischer, I. Thievessen, M. Gregor, B. Fabry, *PLoS Comput. Biol.* **2021**, *17*, e1008364.
[43] Y. Makinen, L. Azzari, A. Foi, *IEEE Trans. Image Process.* **2020**, *29*, 8339.